



Cite this: *RSC Adv.*, 2018, 8, 23981

# Eu<sup>3+/2+</sup> co-doping system induced by adjusting Al/Y ratio in Eu doped CaYAlO<sub>4</sub>: preparation, bond energy, site preference and <sup>5</sup>D<sub>0</sub>–<sup>7</sup>F<sub>4</sub> transition intensity†

Yu Pan,<sup>a</sup> Wenjun Wang,<sup>a</sup> Yuhan Zhu,<sup>a</sup> Haibing Xu,<sup>a</sup> Liguang Zhou,<sup>a</sup> Hyeon Mi Noh,<sup>b</sup> Jung Hyun Jeong,<sup>b</sup> Xiaoguang Liu<sup>\*a</sup> and Ling Li<sup>\*a</sup>

CaY<sub>1-x</sub>Al<sub>1+x</sub>O<sub>4</sub>:2%Eu (x = 0, 0.1, 0.2) phosphors have been synthesized *via* a solid-state reaction process. XRD patterns indicate that they are pure phase. The photoluminescence properties of the CaY<sub>1-x</sub>Al<sub>1+x</sub>O<sub>4</sub>:2%Eu phosphors exhibit both the blue emission of Eu<sup>2+</sup> (4f<sup>6</sup>5d<sup>1</sup>–4f<sup>7</sup>) and red-orange emission of Eu<sup>3+</sup> (<sup>5</sup>D<sub>0</sub>–<sup>7</sup>F<sub>1,2,3,4</sub>) under UV light excitation, which showed that the Eu<sup>3+/2+</sup> co-doping system was obtained by adjusting the Al/Y ratio. Eu<sup>3+</sup> ions can be reduced to Eu<sup>2+</sup> ions when the Al/Y ratio was changed. In this work, the bond energy method was used to determine and explain the mechanism of the site occupation of Eu ions entering the host matrix. Also, the emission spectrum showed an unusual comparable intensity <sup>5</sup>D<sub>0</sub>–<sup>7</sup>F<sub>4</sub> transition peak. The relative intensity of <sup>5</sup>D<sub>0</sub>–<sup>7</sup>F<sub>2</sub> and <sup>5</sup>D<sub>0</sub>–<sup>7</sup>F<sub>4</sub> can be stabilized by changing the relative proportions of Al<sup>3+</sup> and Y<sup>3+</sup>. Furthermore, this was explained by the J–O theory.

Received 24th May 2018  
Accepted 25th June 2018

DOI: 10.1039/c8ra04432e

rsc.li/rsc-advances

## 1. Introduction

Rare-earth ions, as widely used activators, have been playing an irreplaceable role in lighting-emitting diodes (LEDs),<sup>1</sup> due to their abundant emission colors based on the 4f–4f or 5d–4f transitions.<sup>2,3</sup> The luminescence properties of different rare earth ions deliver an explicit comprehension on the internal correlations between them, which is generally determined by electronic configuration of the dopant and dynamic coupling between the dopant and the host lattices.<sup>4,5</sup> The local structure around the rare earth in the crystal lattice also plays an important role in controlling its luminescence performance especially the 4f–5d transitions.<sup>6,7</sup>

Eu ions, including Eu<sup>3+</sup> and Eu<sup>2+</sup>, are the most commonly used activators in phosphor materials among the rare-earth ions.<sup>8–10</sup> Eu<sup>2+</sup> ions emit a tunable color ranging from ultraviolet to red due to its 5d–4f transition.<sup>11,12</sup> The 5d orbit of Eu<sup>2+</sup> is strongly affected by the environment of the crystal, thus the emission of Eu<sup>2+</sup> is strongly influenced by the crystal field.<sup>13</sup> Eu<sup>3+</sup> is one of the most frequently used red-emitting activators,

which mainly shows characteristic emissions resulting from the transitions of <sup>5</sup>D<sub>0</sub>–<sup>7</sup>F<sub>*J*</sub> (*J* = 0, 1, 2, 3, 4).<sup>14,15</sup> However, the partly-forbidden f–f transitions of Eu<sup>3+</sup> have low oscillator strength, resulting in low absorption efficiency and a low color rendering index (CRI). Therefore, it is a promising method to overcome the limitations of Eu<sup>3+</sup> activated phosphors *via* the coexistence of Eu<sup>3+</sup> and Eu<sup>2+</sup> in single phase phosphors.<sup>16</sup>

The Eu<sup>3+/2+</sup> co-doped phosphors can be prepared through a reduction annealing process in a reducing atmosphere such as H<sub>2</sub>, H<sub>2</sub>/N<sub>2</sub> mixture or CO.<sup>16</sup> After that, the Eu<sup>3+/2+</sup> co-doped phosphor can be obtained when Eu<sup>3+</sup> was reduced to Eu<sup>2+</sup> partially not completely. However, it is very difficult to obtain the Eu<sup>3+/2+</sup> co-doped CaYAlO<sub>4</sub> even through conventional high temperature solid-state reaction under a reducing atmosphere. Another extreme example is Eu ion doped CaAl<sub>2</sub>O<sub>4</sub>, in which an abnormal reduction of Eu<sup>3+</sup> → Eu<sup>2+</sup> was observed in monoclinic phase of CaAl<sub>2</sub>O<sub>4</sub>: Eu that calcined in air atmosphere at high temperature.<sup>17,18</sup> Comparing the formula of CaYAlO<sub>4</sub> and CaAl<sub>2</sub>O<sub>4</sub>, the only change is their Al/Y ratio. Herein, we investigated the CaY<sub>1-x</sub>Al<sub>1+x</sub>O<sub>4</sub>:2%Eu system by adjusting the Al/Y ratio. In our work, the phenomenon of the reduction of Eu<sup>3+</sup> to Eu<sup>2+</sup> in CaY<sub>1-x</sub>Al<sub>1+x</sub>O<sub>4</sub> systems was observed, and the bond energy method is adopted to theoretically explain the site preferential occupancy of Eu<sup>2+/3+</sup> in the CaY<sub>1-x</sub>Al<sub>1+x</sub>O<sub>4</sub> systems.

The deviation of its bond energy in different lattice can be compared to determine which site the activators will occupy according to the similar property of chemical bonds and the

<sup>a</sup>Hubei Collaborative Innovation Center for Advanced Organochemical Materials, Ministry-of-Education Key Laboratory for the Synthesis and Applications of Organic Functional Molecules, Hubei University, Wuhan 430062, China. E-mail: liling402431@hotmail.com; Liuxiaoguang402@hotmail.com

<sup>b</sup>Department of Physics, Pukyong National University, Busan 608-737, Korea. E-mail: jhejong@pknu.ac.kr

† Electronic supplementary information (ESI) available. See DOI: 10.1039/c8ra04432e



similar value of their bond energy.<sup>19</sup> The smaller deviation of the bond energy between the host and activators ions, the more easily the lattice site can be replaced by the ion. Therefore, we use this method to solve the site occupancy problem of doping rare earth ions in the matrix. In the previous research, the site preferential occupancy for Eu in Sr<sub>2</sub>V<sub>2</sub>O<sub>7</sub>, Sr<sub>9</sub>Gd(VO<sub>4</sub>)<sub>7</sub> and Sr<sub>2</sub>V<sub>2</sub>O<sub>7</sub>/Sr<sub>9</sub>Gd(VO<sub>4</sub>)<sub>7</sub> phosphors<sup>20</sup> as well as the site occupancy preference of Bi<sup>2+</sup> in β-Ca<sub>2</sub>P<sub>2</sub>O<sub>7</sub> (ref. 21) crystal have been confirmed though the bond energy method.<sup>19</sup> In addition, the bond energy method can connect the relationship between bond energy and preferential occupancy in Eu<sup>3+</sup> doped in CaAl<sub>2</sub>Si<sub>2</sub>O<sub>8</sub> crystal.<sup>22</sup> Our calculated results are in good agreement with the experimental data and the photoluminescence spectra.

In addition, Eu<sup>3+</sup>-doped inorganic phosphors can be used as efficient orange to red emitting phosphors due to the <sup>5</sup>D<sub>0</sub>-<sup>7</sup>F<sub>J</sub> (*J* = 0, 1, 2, 3 and 4) transitions. Most of the phosphors show the dominant emission either <sup>5</sup>D<sub>0</sub> → <sup>7</sup>F<sub>1</sub> (~593 nm) or <sup>5</sup>D<sub>0</sub> → <sup>7</sup>F<sub>2</sub> (~610 nm) transition of Eu<sup>3+</sup> ions. The dominated <sup>5</sup>D<sub>0</sub> → <sup>7</sup>F<sub>4</sub> (~703 nm) transition emission is infrequent. Only some numerable phosphors show that they have stronger intensity of <sup>5</sup>D<sub>0</sub>-<sup>7</sup>F<sub>4</sub> than <sup>5</sup>D<sub>0</sub>-<sup>7</sup>F<sub>1</sub>, such as Sr<sub>0.99</sub>[La<sub>(1-x)</sub>Eu<sub>x</sub>]<sub>1.01</sub>Zn<sub>0.99</sub>O<sub>3.495</sub>,<sup>23</sup> LaBO<sub>3</sub>:Eu<sup>3+</sup>,<sup>24</sup> Na<sub>9</sub>[EuW<sub>10</sub>O<sub>36</sub>]·14H<sub>2</sub>O,<sup>25</sup> Na<sub>2</sub>CaSiO<sub>4</sub>:Eu<sup>3+</sup>,<sup>26</sup> Ca<sub>2</sub>-Ga<sub>2</sub>SiO<sub>7</sub>:Eu<sup>3+</sup>,<sup>27</sup> YAsO<sub>4</sub>:Eu.<sup>28</sup> Similarly, this phenomenon has been found in CaYAlO<sub>4</sub> with Eu doped. But, the stronger emission of <sup>5</sup>D<sub>0</sub>-<sup>7</sup>F<sub>4</sub> disappeared when Eu<sup>3+</sup> and Tb<sup>3+</sup> were co-doped into CaYAlO<sub>4</sub>.<sup>29</sup> However, in our work, the relative intensity of <sup>5</sup>D<sub>0</sub>-<sup>7</sup>F<sub>4</sub> and <sup>5</sup>D<sub>0</sub>-<sup>7</sup>F<sub>2</sub> can be modified by changing the Al<sup>3+</sup> and Y<sup>3+</sup> ions ratios in CaY<sub>1-x</sub>Al<sub>1+x</sub>O<sub>4</sub> and the Judd-Ofelt theory<sup>30</sup> was applied to calculate the radiative properties of the prepared materials.

## 2. Experimental section

### 2.1 Materials and synthesis

A series of CaY<sub>1-x</sub>Al<sub>1+x</sub>O<sub>4</sub>:2%Eu (*x* = 0, 0.1, 0.2, 0.3, 0.4) phosphors was prepared by a traditional high temperature solid-state reaction route using stoichiometric amounts of CaCO<sub>3</sub> (A.R.), Y<sub>2</sub>O<sub>3</sub> (99.99%), Al<sub>2</sub>O<sub>3</sub> (99.99%), Eu<sub>2</sub>O<sub>3</sub> (99.99%) as raw materials, after the reactants were mixed and well-ground in an agate mortar, they were preheated at 1400 °C for 4 hours. Then the mixtures were reground and calcined at 1500 °C for 4 hours. All of CaY<sub>1-x</sub>Al<sub>1+x</sub>O<sub>4</sub>:2%Eu (*x* = 0, 0.1, 0.2, 0.3, 0.4) phosphors prepared under a reducing atmosphere of H<sub>2</sub> (5%) and N<sub>2</sub> (95%). The final power products were obtained after cooling to room temperature and grinding to powder sample.

### 2.2 Characterization

The phase purity of the products was examined by X-ray diffraction (XRD) using a BRUKER D8 ADVANCE powder diffractometer with Cu Kα radiation (0.15405 nm) at room temperature, the diffraction data were collected in 2θ range from 5 to 90°. The UV-vis diffuse reflectance spectra were collected through a Cary 5000 UV-vis-NIR spectrophotometer equipped with a double out-of-plane Littrow monochromator using BaSO<sub>4</sub> as a standard reference. All excitation, emission,

decay spectra and quantum efficiency were measured on an Edinburgh FLS980 combined fluorescence lifetime, a 450 W xenon lamp was used as the excitation source of emission spectra, while a 60 W μF flash lamp with a pulse width of 1.5–3.0 μs was for the measurements of decay curves.

## 3. Result and discussion

### 3.1 Phase characterization

For comparison, the CaYAlO<sub>4</sub>:2%Eu was prepared firstly under a reducing atmosphere of H<sub>2</sub> (5%) and N<sub>2</sub> (95%). The XRD patterns of the CaYAlO<sub>4</sub>:2%Eu together with the Joint Committee on Powder Diffraction Standards (JCPDS) card no. 24-0221 are shown in Fig. 1(a). The XRD patterns of CaYAlO<sub>4</sub>:2%Eu shows that the diffraction peaks of all single samples are matched well with the standard card of CaYAlO<sub>4</sub> (JCPDS: 24-0221), which indicates that the samples are purity phase and doping Eu ions do not cause significant changes to the crystal structure.

In order to get further confirmation and knowledge regarding crystal structure information and sites of CaYAlO<sub>4</sub>:2%Eu, the XRD Rietveld refinement of CaYAlO<sub>4</sub>:2%Eu were performed by the General Structure Analysis System (GASA) program with the single crystallographic data of CaYAlO<sub>4</sub> as the initial model. Fig. 1(b) presents red lines and black lines stand for experimental and calculated patterns, respectively, which matched well with each other. The obtained converged weighted-profiles of *R*<sub>p</sub> = 8.4% and *R*<sub>wp</sub> = 6.1%, which reveals a good quality of fit. As the crystallographic data of CaYAlO<sub>4</sub>:2%Eu shown in Table 1. And Fig. S1† shows the XRD refinements of CaY<sub>0.9</sub>Al<sub>1.1</sub>O<sub>4</sub>:2%Eu and CaY<sub>0.8</sub>Al<sub>1.2</sub>O<sub>4</sub>:2%Eu. This aluminate compound has a tetragonal crystal system with space group *I4/mmm*, *a* = *b* = 3.664 Å, *c* = 11.889 Å, *V* = 159.61 Å<sup>3</sup>. However, the lattice constants of CaYAlO<sub>4</sub>:2%Eu are *a* = *b* = 3.648 Å, *c* = 11.885 Å, which indicates that its crystal constants increase with increasing the concentration of Eu<sup>3+</sup>.

CaYAlO<sub>4</sub> has a tetragonal K<sub>2</sub>NiF<sub>4</sub> structure and belongs to a family of compounds with the general formula ABCO<sub>4</sub>, where A is an alkaline earth cation, B is Y, Sc, or a trivalent rare earth element and C is Al, Ga or a transition metal ion. In the unit cell, as shown in Fig. 1(c), the Ca and Y cations are distributed almost statistically in the nine coordinated sites and Al<sup>3+</sup> ions are coordinated with six oxygen atoms and form the AlO<sub>6</sub> octahedron.

Notably, the (Ca/Y)O<sub>9</sub> polyhedron is closely surrounded by AlO<sub>6</sub> octahedrons to form a cage structure (Fig. S2†). Thus, it can be concluded that the local environment of Ca/Y sites is highly compressed due to the rigid structure of CaYAlO<sub>4</sub>, which gives rise to the difficulty of reduction of Eu<sup>3+</sup> activators. The Lin *et al.* has been reported an effective approach-crystal-site engineering to control Eu<sup>3+</sup> reduced to Eu<sup>2+</sup>.<sup>16</sup> So, a similar way has been used to change the reduction of Eu<sup>3+</sup> doped in CaYAlO<sub>4</sub>.

Compared with Eu<sup>3+</sup>, the smaller ions will replace the Al<sup>3+</sup> site (such B<sup>3+</sup> and Si<sup>4+</sup>), therefore, an artificial defect substitution will be used for Al<sup>3+</sup> doping to CaYAlO<sub>4</sub>. Fig. 2 showed the XRD patterns of CaY<sub>1-x</sub>Al<sub>1+x</sub>O<sub>4</sub>:2%Eu (*x* = 0–0.4). Compared with standard card of CaYAlO<sub>4</sub>, When *x* > 0.2, the XRD pattern diffraction peak appeared a weak miscellaneous



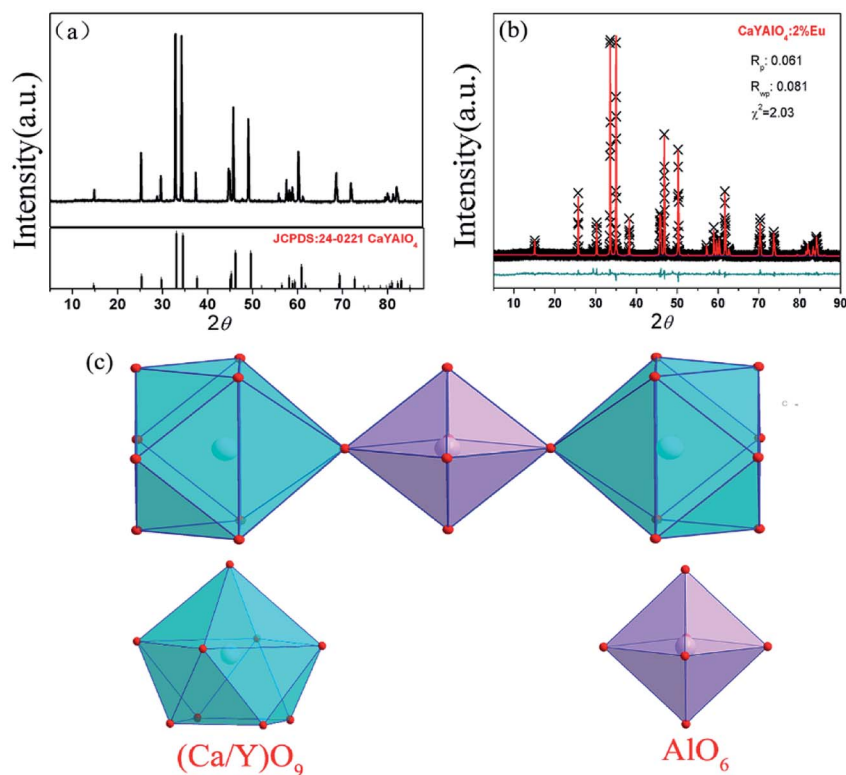


Fig. 1 (a) Powder X-ray diffraction (XRD) patterns of  $\text{CaYAIO}_4:2\% \text{Eu}^{3+}$  and the standard cards of  $\text{CaYAIO}_4$  (JCPDS: 24-0221); (b) experimental (cross), calculated (solid line) and difference (bottom) results of XRD refinements of  $\text{CaYAIO}_4:2\% \text{Eu}^{3+}$ . (c) The crystal structure of  $\text{CaYAIO}_4$ .  $\text{Ca}^{2+}$  or  $\text{Y}^{3+}$  ions are coordinated with nine oxygen atoms to form  $\text{CaO}_9$  or  $\text{YO}_9$  group and  $\text{Al}^{3+}$  ions are coordinated with six oxygen atoms and form the  $\text{AlO}_6$  octahedron.

Table 1 Crystallographic data of  $\text{CaYAIO}_4:0.02\text{Eu}^{3+}$ , as determined by the Rietveld refinement of powder XRD data at room temperature

Atom	Site	x	y	z	Occupancy
Ca1	4e	0.0000	0.0000	0.3604	0.500
Y1	4e	0.0000	0.0000	0.3603	0.490
Eu1	4e	0.0000	0.0000	0.5000	0.010
Al1	2a	0.5000	0.5000	0.5000	1.000
O1	4e	0.5000	0.0000	0.5000	1.000
O2	4e	0.0000	0.0000	0.1686	1.000

peak around  $31^\circ$ , which indicates that a new phase appeared at this time, the diffraction peak at about  $31^\circ$  is described to  $\text{Ca}_3\text{Y}_2\text{O}_6$ , the strongest exact diffraction peak of  $\text{CaAl}_2\text{O}_4$  is at  $30^\circ$  (see Fig. S3†), so the impurity cannot be ascribed to  $\text{CaAl}_2\text{O}_4$ . In addition, the properties of luminescence for Eu ions doped in  $\text{Ca}_3\text{Y}_2\text{O}_6$  crystals aren't detected in research works at present, which indicates that the  $\text{Eu}^{2+}$  or  $\text{Eu}^{3+}$  in  $\text{Ca}_3\text{Y}_2\text{O}_6$  has not any emission at room temperature. When  $x \leq 0.2$ , the diffraction peak of the sample is consistent with the standard card diffraction peak, which means that the  $\text{Al}^{3+}$  actually occupy the  $\text{Y}^{3+}$  within a certain range. Thus, we restricted the  $x$  value to a maximum of 0.20. Table 2 summarizes the lattice parameters and reliability factors of  $\text{CaY}_{1-x}\text{Al}_x\text{O}_4:2\% \text{Eu}$ . In addition, because the  $\text{Al}^{3+}$  ion radius is smaller than that of  $\text{Y}^{3+}$ , the volume of the unit cell will decrease when  $\text{Al}^{3+}$  occupies the  $\text{Y}^{3+}$  site.

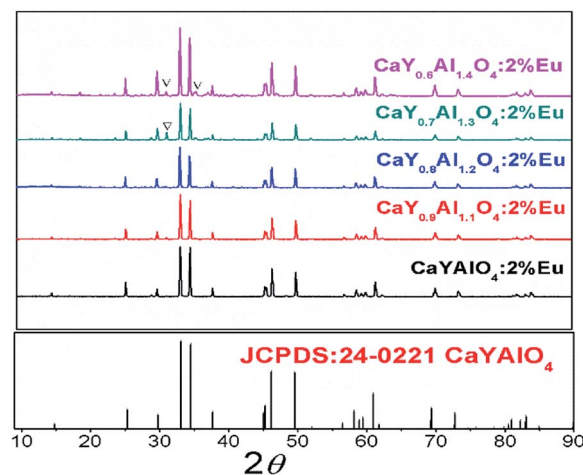


Fig. 2 The powder X-ray diffraction patterns of  $\text{CaY}_{1-x}\text{Al}_x\text{O}_4:2\% \text{Eu}$  ( $x = 0-0.4$ ) and the standard cards of  $\text{CaYAIO}_4$  (JCPDS: 24-0221).

### 3.2 Photoluminescence properties

For Eu doped samples, one can clearly distinguish the different emission bands from the photoluminescence (PL) properties of the two valence states of Eu, *i.e.*, the broad ones are attributed to the parity-allowed  $4f-5d$  transitions of  $\text{Eu}^{2+}$  and the sharp ones are ascribed to the parity-forbidden transitions of  $\text{Eu}^{3+}$  ( ${}^5\text{D}_0 \rightarrow$



Table 2 The lattice parameters and reliability factors of  $\text{CaY}_{1-x}\text{Al}_{1+x}\text{O}_4:2\% \text{Eu}$  ( $x = 0, 0.1, 0.2$ )

Sample	$\text{CaAlYO}_4$	$\text{CaY}_{0.9}\text{Al}_{1.1}\text{O}_4$	$\text{CaY}_{0.8}\text{Al}_{1.2}\text{O}_4$
$R_{\text{wp}}$	0.081	0.092	0.101
$R_{\text{p}}$	0.061	0.071	0.082
$\chi^2$	2.410	2.030	3.890
$a = b$ (Å)	3.664	3.642	3.610
$c$ (Å)	11.889	11.882	11.859
$V$ (Å <sup>3</sup> )	159.61	157.60	154.55

${}^7\text{F}_J, J = 0-4$ ). Fig. 3(a), (c) and (f) illustrate the emission spectra of  $\text{CaY}_{1-x}\text{Al}_{1+x}\text{O}_4:2\% \text{Eu}$  ( $x = 0, 0.1, 0.2$ ) samples under the NUV excitation of 365 nm. When  $x = 0$ , as shown in Fig. 3(b), the photoluminescence excitation (PLE) spectrum monitored at 622 nm reveals a broad band with the peak at 277 nm in the range of 200–350 nm due to the charge transfer band (CTB) from O to the Eu ions, along with some sharp peaks in the range of 350–500 nm related to the 4f–4f transitions of  $\text{Eu}^{3+}$  ions. Under the excitation of 277 or 365 nm, only the sharp f–f

transitions can be found. The sharp emission lines of  $\text{CaYAlO}_4:\text{Eu}$  can be assigned to f–f transition of  $\text{Eu}^{3+}$ , which indicates that  $\text{Eu}^{3+}$  could not be directly reduced to  $\text{Eu}^{2+}$  in  $\text{CaYAlO}_4:\text{Eu}$  system under a reducing atmosphere. All the emissions spectra are intense. The most intense emission at around 622 nm is attributed to the hypersensitive transition  ${}^5\text{D}_0 \rightarrow {}^7\text{F}_2$ , indicating that the  $\text{Eu}^{3+}$  ions mainly occupy the sites without inversion symmetry. The more intense emission at 702 nm is rarely reported. This peak comes from the  ${}^5\text{D}_0 \rightarrow {}^7\text{F}_4$  transition of  $\text{Eu}^{3+}$ . As shown in Fig. S2,† the excitation peaks are similar under the different monitoring wavelength ( $\lambda_{\text{em}} = 592, 621, 702$  nm), which indicates that the emission peaks of  $\text{Eu}^{3+}$  at 592, 621, 702 nm comes from the same site of  $\text{Eu}^{3+}$ .

Fig. 3(b and f) show the emission spectra of  $\text{CaY}_{0.9}\text{Al}_{1.1}\text{O}_4:\text{Eu}$  and  $\text{CaY}_{0.8}\text{Al}_{1.2}\text{O}_4:\text{Eu}$  under the excitation of 365 nm, respectively. It is surprising to find an appearance of a broad band with the peak at 445 nm except for some sharp peaks in the range of 350–500 nm related to the 4f–4f transitions of  $\text{Eu}^{3+}$  ions. Fig. 3(e and h) show the PL spectra of  $\text{CaY}_{0.9}\text{Al}_{1.1}\text{O}_4:\text{Eu}$  and  $\text{CaY}_{0.8}\text{Al}_{1.2}\text{O}_4:\text{Eu}$  under the monitoring wavelength at 445 and

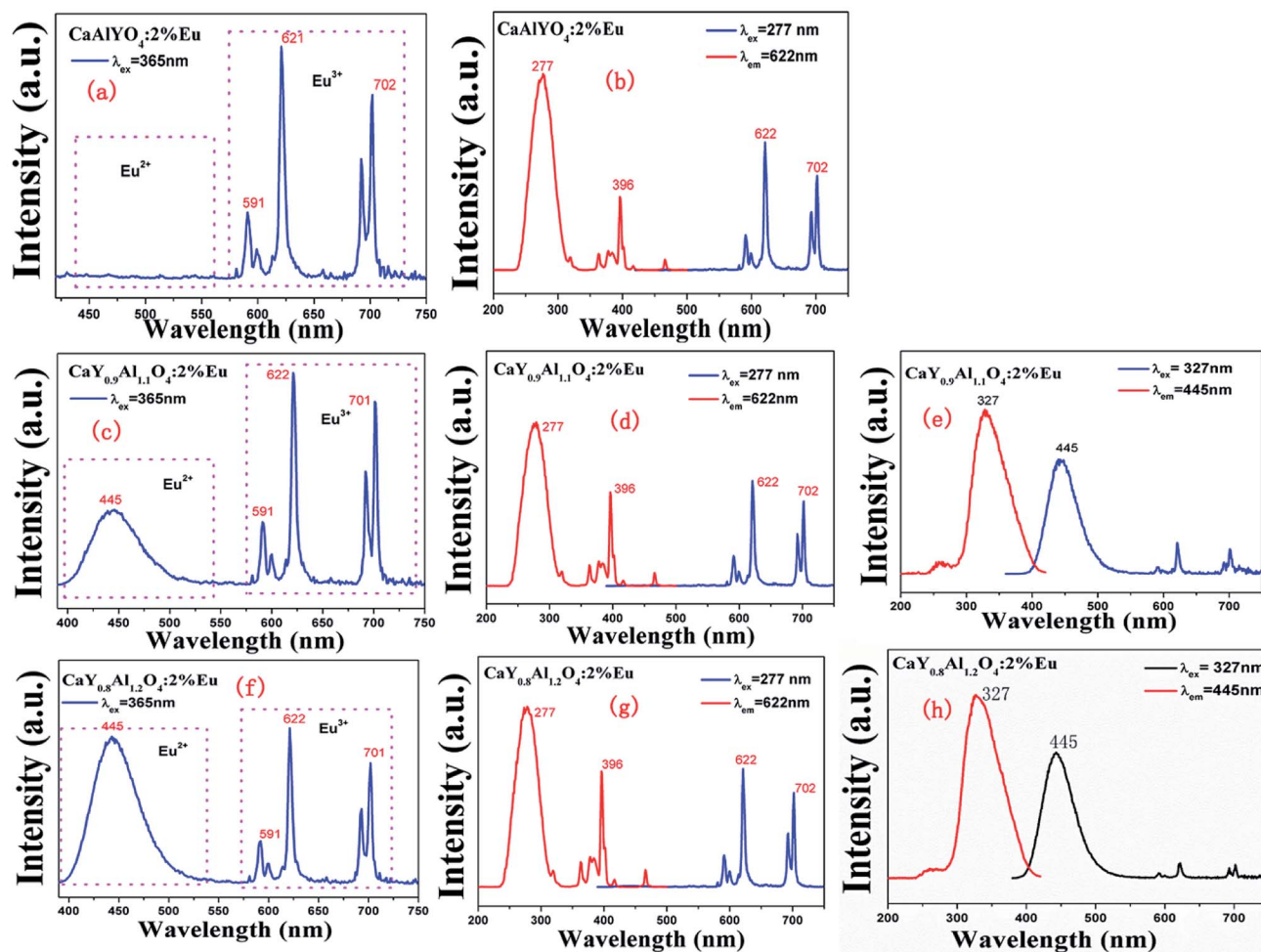


Fig. 3 (a), (c) and (f) are the emission spectra of  $\text{CaYAlO}_4:\text{Eu}$ ,  $\text{CaY}_{0.9}\text{Al}_{1.1}\text{O}_4:\text{Eu}$  and  $\text{CaY}_{0.8}\text{Al}_{1.2}\text{O}_4:\text{Eu}$  under the excitation wavelength at 365 nm, respectively. (b), (d) and (g) are the excitation spectra under the monitoring wavelength at 622 nm and the emission spectra under the excitation wavelength at 277 nm under excitation wavelength of  $\text{CaYAlO}_4:\text{Eu}$ ,  $\text{CaY}_{0.9}\text{Al}_{1.1}\text{O}_4:\text{Eu}$  and  $\text{CaY}_{0.8}\text{Al}_{1.2}\text{O}_4:\text{Eu}$ , respectively. (e) and (h) are the excitation spectra under the monitoring wavelength at 445 nm and the emission spectra under the excitation wavelength at 327 nm of  $\text{CaY}_{0.9}\text{Al}_{1.1}\text{O}_4:\text{Eu}$  and  $\text{CaY}_{0.8}\text{Al}_{1.2}\text{O}_4:\text{Eu}$ , respectively.



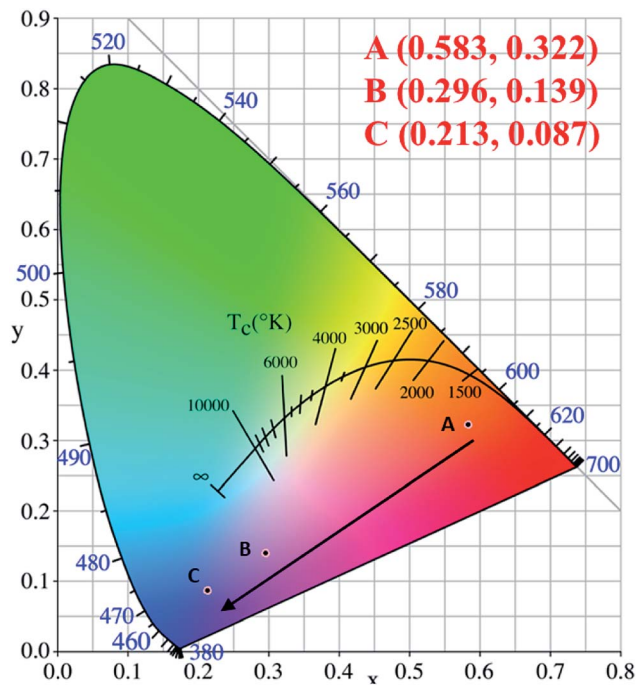


Fig. 4 The corresponding CIE chromaticity diagram for  $\text{CaY}_{1-x}\text{Al}_{1+x}\text{O}_4:2\%\text{Eu}$  ( $x = 0, 0.1, 0.2$ ) under the 365 nm excitation. (A)  $x = 0$ ; (B)  $x = 0.1$ ; (C)  $x = 0.2$ .

the PLE spectra under the excitation wavelength at 327. These correspond to the  $4f^65d^1-4f^7$  transition of  $\text{Eu}^{2+}$ . This indicates that  $\text{Eu}^{3+}$  had been directly reduced to  $\text{Eu}^{2+}$  in  $\text{CaY}_{0.9}\text{Al}_{1.1}\text{O}_4:\text{Eu}$  and  $\text{CaY}_{0.8}\text{Al}_{1.2}\text{O}_4:\text{Eu}$  system under a reducing atmosphere. The luminescence intensity of  $\text{Eu}^{2+}$  increases with increasing  $x$  in  $\text{CaY}_{1-x}\text{Al}_{1+x}\text{O}_4:2\%\text{Eu}$  ( $x = 0, 0.1, 0.2$ ) system (Fig. S4<sup>†</sup>), which can be attributed to the increase of  $x$  value. These results suggest that  $\text{Eu}^{3+}$  is partially transformed to  $\text{Eu}^{2+}$  in  $\text{CaY}_{1-x}\text{Al}_{1+x}\text{O}_4:2\%\text{Eu}$  ( $x = 0, 0.1, 0.2$ ).

The corresponding CIE chromaticity diagram for  $\text{CaY}_{1-x}\text{Al}_{1+x}\text{O}_4:2\%\text{Eu}$  ( $x = 0, 0.1, 0.2$ ) has been shown in Fig. 4. The points A, B and C stand for the CIE coordinate position when  $x = 0, 0.1$  and  $0.2$ , respectively. With increasing of the Al/Y ratio in  $\text{CaY}_{1-x}\text{Al}_{1+x}\text{O}_4:2\%\text{Eu}$ , the emission color changed from A (0.583, 0.322) red to C (0.213, 0.083) blue.

The diffuse reflectance in the UV-vis region was used to calculate the experimental band-gap value of  $\text{CaY}_{1-x}\text{Al}_{1+x}\text{O}_4:\text{Eu}^{3+}$  ( $x = 0, 0.1, 0.2$ ). Fig. 5 illustrates the diffuse reflectance of  $\text{CaY}_{1-x}\text{Al}_{1+x}\text{O}_4:2\%\text{Eu}$  ( $x = 0, 0.1, 0.2$ ). The results show that the samples begin to exhibit low reflectance below 330 nm due to the high radiation absorption. This behavior is assigned to the edge absorption, corresponding to the electronic transition from the valence band to the conduction band of  $\text{CaYAlO}_4$ . The matrix of yttrium aluminate and calcium shows optical transparency in the visible region between 330 and 750 nm, making it a candidate for applications in photonic devices.

In Fig. 5b–d, the  $(h\nu F(R_\infty))^2$  of  $\text{CaY}_{1-x}\text{Al}_{1+x}\text{O}_4:2\%\text{Eu}$  ( $x = 0, 0.1, 0.2$ ) was plotted against the  $(h\nu)$  using the Kubelka–Munk function.<sup>31</sup> The following relational expression proposed by Tauc, Davis, and Mott is used:<sup>32,33</sup>

$$[\alpha h\nu]^n = A(h\nu - E_g) \quad (1)$$

where  $h$  is Planck's constant,  $\nu$  is frequency of vibration,  $\alpha$  is absorption coefficient,  $E_g$  is band gap, and  $A$  is proportional constant.  $h\nu$  represents the energy per photon,  $E_g$  is the value of the band gap,  $n = 1/2$  means a indirect allowed transition, 2 represents a direct allowed transition,  $3/2$  stands for a direct forbidden transition, or 3 indicates as indirect forbidden transition. Since the direct allowed transition is used in the experiment,  $n = 2$  is used for these samples.

The acquired diffuse reflectance spectra of  $\text{CaY}_{1-x}\text{Al}_{1+x}\text{O}_4:2\%\text{Eu}$  ( $x = 0, 0.1, 0.2$ ) in Fig. 5 are converted to Kubelka–Munk equation:<sup>32,34</sup>

$$F(R_\infty) = \frac{(1 - R_\infty)^2}{2R_\infty} \quad (2)$$

where  $R_\infty$  is the diffuse reflectance of the layer relative to the standard. Thus, the vertical axis is converted to quantity  $F(R_\infty)$ , which is proportional to the absorption coefficient  $\alpha$ . The  $\alpha$  in the Tauc equation is substituted with  $F(R_\infty)$ . Thus, in the actual experiment, the relational expression (1) becomes:<sup>23,34</sup>

$$(h\nu F(R_\infty))^2 = C(h\nu - E_g) \quad (3)$$

where  $C$  is a proportional constant. Using the Kubelka–Munk function, the was plotted against the  $h\nu$ . The curves that plots the value of  $(h\nu - (h\nu F(R_\infty))^2)$  on the horizontal axis  $h\nu$  and vertical axis  $(h\nu F(R_\infty))^2$  are drawn in Fig. 5(b–d). Here, the unit for  $h\nu$  is eV (electron volts), and its relationship to the wavelength  $\lambda$  (nm) becomes  $h\nu = 1239.7/\lambda$ . A red lines are drawn tangent to the point of inflection on the black curves. The values associated with the point of intersection of the lines tangent to the plotted curve inflection point with the horizontal axis ( $h\nu$  axis) becomes the band gap  $E_g$  value. Their band gaps of  $\text{CaY}_{1-x}\text{Al}_{1+x}\text{O}_4:2\%\text{Eu}$  ( $x = 0, 0.1, 0.2$ ) are 4.10, 4.10 and 4.11 eV. The results show that a significant changing cannot be found in the band-gap edge with increasing value of  $x$ . In fact, the R. V. Perrella's<sup>34</sup> reported that the difference of energy band-gap between samples doped with 1 and 10 mol% of  $\text{Eu}^{3+}$  is in the order of magnitude of the phonon energy of the lattice, the  $\text{Eu}^{3+}$  substitute  $\text{Y}^{3+}$  cannot change the band gap. Here, when the  $x$  increases and cause the band gap also unchanged, so we infer that  $\text{Al}^{3+}$  also substitute the  $\text{Y}^{3+}$  site rather than  $\text{Ca}^{2+}$  site.

The decay curves of  $\text{Eu}^{3+}$  shown in Fig. 6a–c are accurately fitted using the following single-exponential equation:

$$I(t) = I_0 \exp\left(-\frac{t}{\tau}\right) \quad (4)$$

where  $I_t$  and  $I_0$  are the intensity at time  $t$  and time zero, respectively, the  $\tau$  is the lifetime. When under the excitation wavelength of 394 nm, the lifetimes of  $\text{Eu}^{3+}$  in  $\text{CaYAlO}_4:\text{Eu}$ ,  $\text{CaY}_{0.9}\text{Al}_{1.1}\text{O}_4:\text{Eu}$  and  $\text{CaY}_{0.8}\text{Al}_{1.2}\text{O}_4:\text{Eu}$  are 1.198 ms, 1.190 ms and 1.201 ms, respectively.

The decay curves of  $\text{Eu}^{2+}$  in Fig. 6d and e are accurately fitted well to a second-order exponential decay model based on the following formula:



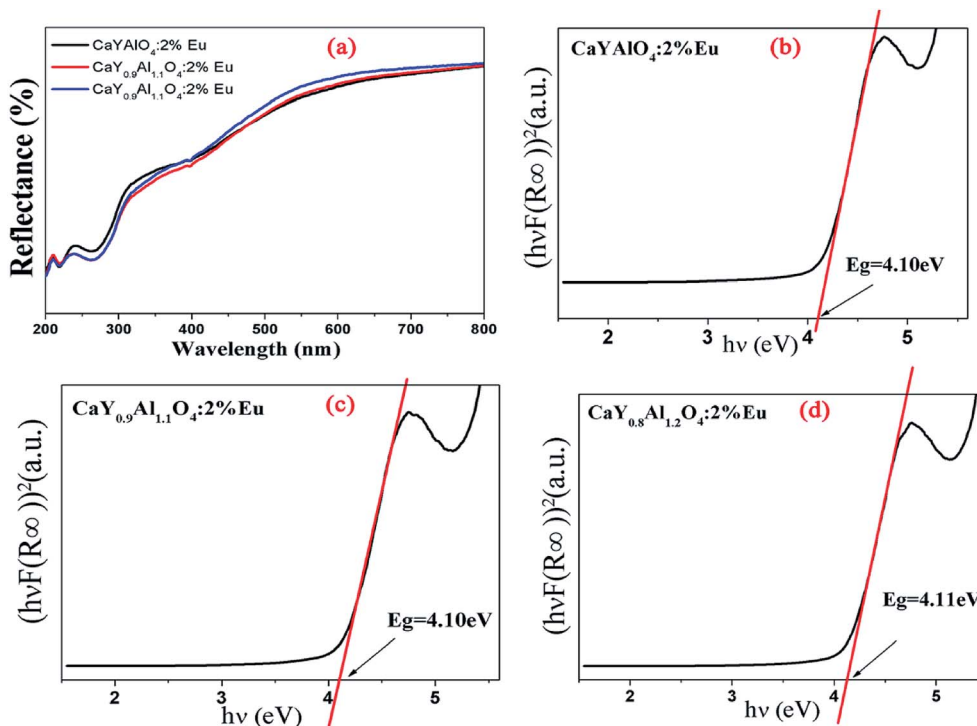


Fig. 5 (a) Diffuse reflectance of  $\text{CaY}_{1-x}\text{Al}_{1+x}\text{O}_4:2\% \text{Eu}$  ( $x = 0, 0.1, 0.2$ ). (b), (c) and (d): The  $(hvF(R_\infty))^2$  was plotted against the  $(hv)$  using the Kubelka–Munk function.

$$I(t) = A_1 \exp\left(-\frac{t}{\tau_1}\right) + A_2 \exp\left(-\frac{t}{\tau_2}\right) \quad (5)$$

$$\tau = \frac{(A_1\tau_1^2 + A_2\tau_2^2)}{(A_1\tau_1 + A_2\tau_2)} \quad (6)$$

where  $I(t)$  is the luminescence intensity at times  $t$ .  $A_1$  and  $A_2$  are fitting constants,  $\tau_1$  and  $\tau_2$  are exponential component of the decay time and  $t$  is the time, respectively. The average decay time can be described by the following formula:

According to the equation, the lifetimes of  $\text{Eu}^{2+}$  in  $\text{CaY}_{0.9}\text{Al}_{1.1}\text{O}_4:\text{Eu}$  and  $\text{CaY}_{0.8}\text{Al}_{1.2}\text{O}_4:\text{Eu}$  are calculated to be 1.07 ns and 1.14 ns, respectively.

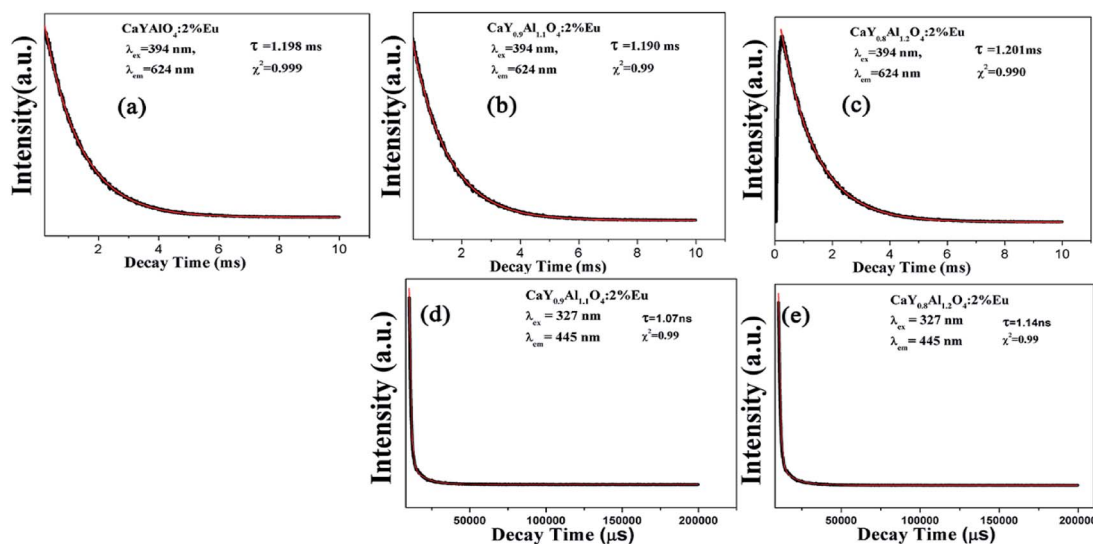


Fig. 6 (a), (b) and (c) are the decay curves of  $\text{Eu}^{3+}$  ions in  $\text{CaY}_{1-x}\text{Al}_{1+x}\text{O}_4:2\% \text{Eu}$  ( $x = 0, 0.1, 0.2$ ) ( $\lambda_{\text{ex}} = 394 \text{ nm}$ ,  $\lambda_{\text{em}} = 624 \text{ nm}$ ). The (d) and (e) are the decay curves of  $\text{Eu}^{2+}$  ions in the  $\text{CaY}_{1-x}\text{Al}_{1+x}\text{O}_4:2\% \text{Eu}$  ( $x = 0.1, 0.2$ ) sample ( $\lambda_{\text{ex}} = 327 \text{ nm}$ ,  $\lambda_{\text{em}} = 445 \text{ nm}$ ).



### 3.3 Bond energy method and preferential occupancy of Eu ions

The dopant occupancy in the matrix can be determined by comparing the deviation of its bond energy in different lattice location. The similar value of the deviation for its bond energy, the more stable the dopants in matrix are. Thus, to determine which site  $\text{Eu}^{3+}$  and  $\text{Eu}^{2+}$  will occupy, the bond-energy method has been used to study to the local structure  $\text{Eu}^{3+}/\text{Eu}^{2+}$  in  $\text{CaYAlO}_4$  crystals. The bond energy of different dopants in  $\text{CaYAlO}_4$  crystallographic frame can be estimated through the following equation:<sup>19,21,22</sup>

$$E_{\text{Ca/Y/Al-O}} = J \exp\left(\frac{d_0 - d_{\text{Ca/Y/Al-O}}}{0.37}\right) \left(\frac{V_{\text{Ca/Y/Al}}}{V_{\text{Eu}}}\right) \quad (7)$$

$V_{\text{Eu}}$  is valence state of Eu (including +2 or +3), both  $J$  and  $d_0$  are constant usually they can be found in reference.  $E_{\text{Ca/Y/Al-O}}$  is mean the bond energy of Ca-O, Y-O or Al-O. In the case of pure  $\text{CaYAlO}_4$  crystals without any dopant,  $V_{\text{Ca/Y/Al}}/V_{\text{Eu}}$  is equal to 1. The eqn (7) can be expressed as:<sup>19,21,22</sup>

$$E_{\text{Ca/Y/Al-O}} = J \exp\left(\frac{d_0 - d_{\text{Ca/Y/Al-O}}}{0.37}\right) \quad (8)$$

and if is not equal to 1, then it means the valence state affects the crystal bond energy effectively.

It is assumed that the  $\text{Eu}^{3+}-\text{O}^{2-}$  bonds have the similar bond lengths as Ca/Y/Al-O bonds when the dopant substitutes Ca/Y/Al cations. In this regard, the value of various un-doped and doped  $\text{CaYAlO}_4$  crystals can be evaluated. The displacement of dopants leads to a large variation of the crystal composition and bond energy, which may affect not only the crystal properties but also the crystal stability. In such a case, it is convenient to measure the variation of bond energy by the following expression when the Eu locates at Ca/Y/Al sites. Based on chemical viewpoint, the dopants preferentially occupy the sites with smaller alterations of bond energy, the sites with smaller absolute values can be expressed as below,<sup>19,21,22</sup>

$$\Delta E_{\text{Eu}}^{\text{Ca/Y/Al}} = |E_{\text{Ca/Y/Al-O}} - E_{\text{Eu-O}}| \quad (9)$$

Here  $\Delta E_{\text{Eu}}^{\text{Ca/Y/Al}}$  is the variation of bond energy when the Eu locates at Ca/Y/Al sites. Based on chemical viewpoint, the dopants preferentially occupy the sites with smaller deviation of bond energy ( $E_{\text{Ca/Y/Al-O}}$ ), the sites with smaller absolute values of  $\Delta E_{\text{Eu}}^{\text{Ca/Y/Al}}$ .

According to the bond energy method, the values of bond energy of  $\text{CaY}_{1-x}\text{Al}_{1+x}\text{O}_4:2\% \text{Eu}$  ( $x = 0.1, 0.2$ ) have been shown in Table 3. The order of variation of bond energy under the assumption that  $\text{Ca}^{2+}/\text{Y}^{3+}/\text{Al}^{3+}$  ions are substituted by  $\text{Eu}^{3+}$  is  $\Delta E_{\text{Eu}^{3+}}^{\text{Y}} (3.236 \text{ kcal mol}^{-1}) < \Delta E_{\text{Eu}^{3+}}^{\text{Ca}} (6.533 \text{ kcal mol}^{-1}) \ll \Delta E_{\text{Eu}^{3+}}^{\text{Al}} (118.789 \text{ kcal mol}^{-1})$ , which means that  $\text{Eu}^{3+}$  will preferentially replaces  $\text{Y}^{3+}$ . The calculation result is consistent with the experiment. In addition, the order of variation of bond energy  $\text{Eu}^{2+}$  substituted  $\text{Y}^{3+}$ ,  $\text{Ca}^{2+}$  and  $\text{Al}^{3+}$  is  $\Delta E_{\text{Eu}^{2+}}^{\text{Y}} (12.386 \text{ kcal mol}^{-1}) \approx \Delta E_{\text{Eu}^{2+}}^{\text{Ca}} (12.633 \text{ kcal mol}^{-1}) \ll \Delta E_{\text{Eu}^{2+}}^{\text{Al}} (67.149 \text{ kcal mol}^{-1})$ , which means that the site of  $\text{Ca}^{2+}$  and  $\text{Y}^{3+}$  could be replaced by  $\text{Eu}^{2+}$  equally. Considering the valence of  $\text{Eu}^{2+}$ , we can determine that the  $\text{Eu}^{2+}$  is preferentially occupied the site of  $\text{Ca}^{2+}$ .

### 3.4 The ${}^5\text{D}_0-{}^7\text{F}_4$ emission for $\text{CaY}_{1-x}\text{Al}_{1+x}\text{O}_4:2\% \text{Eu}$ ( $x = 0, 0.1, 0.2$ )

The emission spectrum showed an unusual comparable intensity  ${}^5\text{D}_0-{}^7\text{F}_4$  transition peak. The relative intensity of  ${}^5\text{D}_0-{}^7\text{F}_2$  and  ${}^5\text{D}_0-{}^7\text{F}_4$  can be stable by changing the relative proportions of  $\text{Al}^{3+}$  and  $\text{Y}^{3+}$ . To gain some insight into the nature of the luminescence behavior of  $\text{Al}^{3+}$  ions in crystal  $\text{CaYAlO}_4:2\% \text{Eu}$  powders, the Judd-Ofelt model was applied to the determination of spontaneous emission coefficients. The intensity parameters  $\Omega_2$  and  $\Omega_4$  were determined from luminescence spectra using the method proposed by Kodaira *et al.*<sup>28,35</sup>

The emission intensity,  $I = \hbar\omega AN$ , is expressed in terms of the surface under the emission curve, where  $\hbar\omega$  is the transition energy,  $N$  is the population of the emitting level ( ${}^5\text{D}_0$ ) and the Einstein's coefficient of spontaneous emission can be given by<sup>25</sup>

$$A_{0-\lambda} = \frac{4e^2\omega^3}{3\hbar c^3} \chi \sum_{\lambda=2,4} \Omega_{\lambda} \langle {}^5\text{D}_0 || U^{(\lambda)} || {}^7\text{F}_J \rangle^2 \quad (10)$$

where  $\chi = n_0(n_0^2 + 2)^2/9$  is a Lorentz local field correction. The square reduced matrix elements  $\langle {}^5\text{D}_0 || U^{(2)} || {}^7\text{F}_2 \rangle^2 = 0.003289$ ;  $\langle {}^5\text{D}_0 || U^{(2)} || {}^7\text{F}_4 \rangle^2 = 0.002365$  in eqn (10) and an average index of refraction equal to 1.5 was used.<sup>36</sup> In this case the  $A_{0-\lambda}$  values are obtained by using the relation:<sup>25,37</sup>

$$A_{0-\lambda} = A_{0-1} \frac{S_{0-\lambda}}{S_{0-1}} \frac{\sigma_{\lambda}}{\sigma_1} \quad (11)$$

where  $S_{0-\lambda}$  is the area under the curve related to the  ${}^5\text{D}_0-{}^7\text{F}_{\lambda}$  transition obtained from the spectral data,  $\sigma_{\lambda}$  is the energy barycenter of the  $0-\lambda$  transition and  $A_{0-1}$  is the Einstein's coefficient for the  $0-1$  magnetic dipole transition. The  $A_{0-1}$  value is estimated to be around of  $50 \text{ s}^{-1}$ .

The lifetime ( $\tau$ ), non-radiative ( $A_{\text{nrad}}$ ) and radiative ( $A_{\text{rad}}$ ) rates are related through the following equation:<sup>35</sup>

$$A_{\text{tot}} = \frac{1}{\tau} = A_{\text{rad}} + A_{\text{nrad}} \quad (12)$$

where the radiative ( $A_{\text{rad}}$ ) rates was obtained by summing over the radiative rates  $A_{0-J}$  for each  ${}^5\text{D}_0-{}^7\text{F}_J$  transitions. It can be given by:<sup>35</sup>

$$A_{\text{rad}} = \sum_J A_{0-J} \quad (13)$$

The emission quantum efficiency of the emitting  ${}^5\text{D}_0$  level is given by:<sup>35</sup>

$$\eta = \frac{A_{\text{rad}}}{A_{\text{rad}} + A_{\text{nrad}}} \quad (14)$$

The values of the  $\Omega_2$  and  $\Omega_4$  parameters as well as other quantities derived from analysis of the luminescence spectra of  $\text{Al}^{3+}$  replace the  $\text{Y}^{3+}$  in  $\text{CaYAlO}_4$  are given in Table 4.

Table 4 shows intensity parameters  $\Omega_2$  and  $\Omega_4$ .  $\Omega_{\lambda}$  is the emission intensity parameters;  $\Omega_2$  is the emission intensity parameter of  ${}^5\text{D}_0-{}^7\text{F}_2$ .  $\Omega_4$  means the emission intensity parameter of  ${}^5\text{D}_0-{}^7\text{F}_4$ . Here, the  $\Omega_2$  intensity parameter values are higher than  $\Omega_4$  for  $\text{CaY}_{1-x}\text{Al}_{1+x}\text{O}_4:2\% \text{Eu}$  ( $x = 0, 0.1, 0.2$ ). The



**Table 3** The bond parameters of the central atom and values of bond energy when  $\text{Eu}^{3+}$  locates at Ca, Y, and Al sites in  $\text{CaYAlO}_4$ . All of the bond energy unit are  $\text{kcal mol}^{-1}$

Central atom	Coordination atom	Count	$d$ (Å)	$E_{\text{M-O}}$	$E_{\text{Eu}^{3+}}$	$E_{\text{Eu}^{2+}}$	$\Delta E_{\text{Eu}^{3+}}^{\text{M}}$	$\Delta E_{\text{Eu}^{2+}}^{\text{M}}$
Ca1	O2	1×	2.3013	51.291	39.457	28.407	6.533	12.633
	O1	4×	2.5152	28.772	22.133	15.935		
	O2	4×	2.6125	22.119	17.015	12.250		
Al1	O1	4×	1.8375	73.757	207.306	149.253	118.784	67.149
	O2	2×	1.9866	49.294	138.549	99.750		
	O2	1×	2.3013	65.045	59.186	42.611		
Y1	O2	1×	2.3013	65.045	59.186	42.611	3.236	12.385
	O1	4×	2.5152	36.488	33.200	23.903		
	O2	4×	2.6125	28.050	25.523	18.376		

**Table 4** Decay rates of radiative ( $A_{\text{rad}}$ ), nonradiative ( $A_{\text{nrad}}$ ), and total ( $A_{\text{tot}}$ ) processes of  ${}^5\text{D}_0\text{--}{}^7\text{F}_j$  transitions, luminescence lifetime ( $\tau$ ), intensity parameters ( $\Omega_2$ ,  $\Omega_4$ ), quantum efficiencies ( $\eta$ ) and actual quantum efficiency ( $\eta_a$ ) of  $\text{CaY}_{1-x}\text{Al}_{1+x}\text{O}_4:2\%\text{Eu}$

Samples	$A_{\text{rad}}$	$A_{\text{nrad}}$	$A_{\text{tot}}$	$\tau$	$\Omega_2$	$\Omega_4$	$\eta$	$\eta_a$
$\text{CaYAlO}_4$	409	427	836	1.198	4.12	2.97	0.489	47.69%
$\text{CaY}_{0.9}\text{Al}_{1.1}\text{O}_4$	406	434	840	1.190	3.99	3.09	0.483	50.42%
$\text{CaY}_{0.8}\text{Al}_{1.2}\text{O}_4$	403	429	832	1.201	3.91	3.10	0.484	55.43%

$\Omega_2$  parameter depends rather on the lower rank components of crystal field and dynamic coupling interactions, while the  $\Omega_4$  parameter depend rather on the corresponding higher components. It suggests that site symmetry occupied by  $\text{Eu}^{3+}$  ions does not have a character of centrosymmetric chemistry environment considering that the  ${}^5\text{D}_0\text{--}{}^7\text{F}_2$  transitions is formally forbidden due to the electric dipole selection rule. Meanwhile, it has been commented in literature that the luminescence spectra of compounds with  $\text{D}_{4d}$  (see Fig. 1(c)) symmetry are often dominated by the  ${}^5\text{D}_0\text{--}{}^7\text{F}_4$  transition of  $\text{Eu}^{3+}$  because of the absence of central symmetry. An undistorted square anti-prism has  $\text{D}_{4d}$  symmetry, so a site with symmetry lower than  $\text{D}_{4d}$  but the coordination polyhedron close to a square anti-prism, is expected to have an intense  ${}^5\text{D}_0\text{--}{}^7\text{F}_4$  transition. In  $\text{CaY}_{1-x}\text{Al}_{1+x}\text{O}_4:2\%\text{Eu}$ ,  $\text{Eu}^{3+}$  is nine-fold coordinated, this coordination polyhedron can be regarded as close to mono-capped square-anti-prism. As a result, in this compound the  ${}^5\text{D}_0\text{--}{}^7\text{F}_4$  transition is less intense than the  ${}^5\text{D}_0\text{--}{}^7\text{F}_2$  transition but much more intense than  ${}^5\text{D}_0\text{--}{}^7\text{F}_1$  magnetic dipole transition. The same remarks have also been for  $\text{LaBO}_3:\text{Eu}^{3+}$ ,  $[\text{Eu}(\text{DOTA})(\text{H}_2\text{O})]^-$  and  $\text{Sr}_{0.99}\text{La}_{1.01}\text{Zn}_{0.99}\text{O}_{3.495}:\text{Eu}^{3+}$ . In addition, the values of  $\Omega_4/\Omega_2$  is 0.72, 0.77, 0.79 for  $\text{CaY}_{1-x}\text{Al}_{1+x}\text{O}_4:2\%\text{Eu}$  ( $x = 0, 0.1, 0.2$ ) respectively, which indicated the  ${}^5\text{D}_0\text{--}{}^7\text{F}_4$  emission can be enhanced by properly adjusting the Al/Y ratio, at the same time it does not change the quantum efficiency ( $\eta$ ). The quantum efficiency ( $\eta_a$ ) measured by the integrating sphere is nearly the result by calculation.

## 4. Conclusions

A series of  $\text{CaY}_{1-x}\text{Al}_{1+x}\text{O}_4:2\%\text{Eu}^{3+}$  ( $x = 0, 0.1, 0.2, 0.3$ ) phosphors have been identified. The powder XRD patterns and Rietveld

refinement reveal that  $\text{CaY}_{1-x}\text{Al}_{1+x}\text{O}_4:2\%\text{Eu}^{3+}$  have a tetragonal crystal structure with the space group  $I4/mmm$  (No. 139). The photoluminescence property of the  $\text{CaY}_{1-x}\text{Al}_{1+x}\text{O}_4:2\%\text{Eu}$  ( $x = 0, 0.1, 0.2$ ) phosphors exhibit both blue emission of  $\text{Eu}^{2+}$  ( $4f^65d^1\text{--}4f^7$ ) and red-orange emission of  $\text{Eu}^{3+}$  ( ${}^5\text{D}_0\text{--}{}^7\text{F}_{1,2,3,4}$ ) under UV light excitation, which showed that  $\text{Eu}^{3+/2+}$  co-doping system was obtained by adjusting Al/Y ratio.  $\text{Eu}^{3+}$  ions can be reduced to  $\text{Eu}^{2+}$  ions when Al/Y ratio was changed. Calculated by the bond-energy theory found that  $\text{Eu}^{3+}$  takes priority over the  $\text{Y}^{3+}$  site, in addition, the site of  $\text{Ca}^{2+}$  and  $\text{Y}^{3+}$  all can be occupied by  $\text{Eu}^{2+}$ . Considering the valence of  $\text{Eu}^{2+}$ , it can determine that the  $\text{Eu}^{2+}$  is preferentially occupied the site of  $\text{Ca}^{2+}$ . The Judd–Ofelt model was applied to the determination of spontaneous emission coefficients. The intensity parameters  $\Omega_2$  and  $\Omega_4$  were determined from luminescence spectra.

## Conflicts of interest

There are no conflicts to declare.

## Acknowledgements

This work is financially supported by the National Natural Science Foundations of China (Grant no. 21301053 and 21571165) and Hubei Natural Science Foundations from Science and Technology Department of Hubei Province (2018CFB517). This research was supported by the Basic Science Research Program through the National Research Foundation of Korea (NRF) funded by the Ministry of Science, ICT and Future Planning (No. 2018R1A2B6005179). “ $\text{Eu}^{3+/2+}$  co-doping system induced by adjusting Al/Y ratio in  $\text{CaY}_{1-x}\text{Al}_{1+x}\text{O}_4:2\%\text{Eu}$ : preparation, bond energy, site preferential and  ${}^5\text{D}_0\text{--}{}^7\text{F}_4$  transition intensity” is supplied by the Functional Phosphor Bank at Pukyong National University.

## Notes and references

- S. Liu, G. Zhao, H. Ying, J. Wang and G. Han, *Opt. Mater.*, 2008, **31**, 47–50.
- T. Selvalakshmi, S. Sellaiyan, A. Uedono and A. Chandra Bose, *Mater. Chem. Phys.*, 2015, **166**, 73–81.
- K. Biswas, A. D. Sontakke, R. Sen and K. Annapurna, *J. Fluoresc.*, 2012, **22**, 745–752.



- 4 L. Yang, Y. Wan, Y. Huang, X. Wang, H. Cheng and H. J. Seo, *Mater. Lett.*, 2016, **172**, 23–26.
- 5 B. Wiendlocha, S. P. Kim, Y. Lee, B. He, G. Lehr, M. G. Kanatzidis, D. T. Morelli and J. P. Heremans, *Phys. Chem. Chem. Phys.*, 2017, **19**, 9606–9616.
- 6 P. L. Roeder, D. MacArthur, X. P. Ma, G. R. Palmer and A. N. Mariano, *Am. Mineral.*, 1987, **72**, 801–811.
- 7 Y. Su, L. Li and G. Li, *Chem. Mater.*, 2008, **20**, 6060–6067.
- 8 H. You and C. Shi, *Chin. Sci. Bull.*, 1996, **41**, 123–126.
- 9 J.-G. Kang, J.-S. Jung, J.-P. Hong, S.-J. Won, Y. Sohn and C. K. Rhee, *J. Phys.: Condens. Matter*, 2001, **13**, 2835–2843.
- 10 Z. Pei, Q. Zeng and Q. Su, *J. Phys. Chem. Solids*, 1999, **61**, 9–12.
- 11 J. S. Zhong, H. B. Gao, Y. J. Yuan, L. F. Chen, D. Q. Chen and Z. G. Ji, *J. Alloys Compd.*, 2018, **735**, 2303–2310.
- 12 Z. Jiang, X. Yu, J. Gou, L. Duan, X. Su, G. Fan and Y. Duan, *J. Mater. Sci.: Mater. Electron.*, 2017, **28**, 3630–3636.
- 13 H. Chen, X. Huang and W. Huang, *Chin. J. Phys.*, 2016, **54**, 931–939.
- 14 K. Li, H. Lian, M. Shang and J. Lin, *Dalton Trans.*, 2015, **44**, 20542–20550.
- 15 Y. Wang, J. Ding, Y. Li, L. Yang, X. Ding and Y. Wang, *RSC Adv.*, 2016, **6**, 42618–42626.
- 16 Y. Zhang, X. Li, K. Li, H. Lian, M. Shang and J. Lin, *ACS Appl. Mater. Interfaces*, 2015, **7**, 2715–2725.
- 17 K. Kumar, A. K. Singh and S. B. Rai, *Spectrochim. Acta, Part A*, 2013, **102**, 212–218.
- 18 Y. Zhang, J. Chen, C. Xu, Y. Li and H. J. Seo, *Phys. B*, 2015, **472**, 6–10.
- 19 Y. He and D. Xue, *J. Phys. Chem. C*, 2007, **111**, 13238–13243.
- 20 L. Li, W. Wang, Y. Pan, Y. Zhu, X. Liu, H. M. Noh, B. K. Moon, B. C. Choi and J. H. Jeong, *RSC Adv.*, 2018, **8**, 1191–1202.
- 21 L. Li, J. Cao, B. Viana, S. Xu and M. Peng, *Inorg. Chem.*, 2017, **56**, 6499–6506.
- 22 L. Li, Y. Pan, W. Wang, Y. Zhu, W. Zhang, H. Xu, L. Zhou and X. Liu, *J. Alloys Compd.*, 2018, **731**, 496–503.
- 23 R. Shi, B. Li, C. Liu and H. Liang, *J. Phys. Chem. C*, 2016, **120**, 19365–19374.
- 24 Z. Babakhanova, M. Aripova and E. Bernardo, *Glass Ceram.*, 2016, **73**, 124–127.
- 25 R. A. Sa Ferreira, S. S. Nobre, C. M. Granadeiro, H. I. S. Nogueira, L. D. Carlos and O. L. Malta, *J. Lumin.*, 2006, **121**, 561–567.
- 26 M. Xie, Y. Li and R. Li, *J. Lumin.*, 2013, **136**, 303–306.
- 27 G. K. Behrh, R. Gautier, C. Latouche, S. Jobic and H. Serier-Brault, *Inorg. Chem.*, 2016, **55**, 9144–9146.
- 28 A. Strzep, A. Watras, K. Zawisza, P. Boutinaud and R. J. Wigiłusz, *Inorg. Chem.*, 2017, **56**, 10914–10925.
- 29 D. Geng, G. Li, M. Shang, C. Peng, Y. Zhang, Z. Cheng and J. Lin, *Dalton Trans.*, 2012, **41**, 3078–3086.
- 30 S. Lv, Y. Wang, Z. Zhu, Z. You, J. Li, S. Gao, H. Wang and C. Tu, *Appl. Phys. B: Lasers Opt.*, 2014, **116**, 83–89.
- 31 J. Chen, W. Zhao, J. Wang and N. Wang, *J. Mater. Sci.: Mater. Electron.*, 2016, **27**, 237–244.
- 32 Y. Su, L. Peng, C. Du and X. Wang, *J. Phys. Chem. C*, 2012, **116**, 15–21.
- 33 Y. Su, L. Peng, J. Guo, S. Huang, L. Lv and X. Wang, *J. Phys. Chem. C*, 2014, **118**, 10728–10739.
- 34 R. V. Perrella, C. S. Nascimento Jr, M. S. Goes, E. Pecoraro, M. A. Schiavon, C. O. Paiva-Santos, H. Lima, M. A. Couto dos Santos, S. J. L. Ribeiro and J. L. Ferrari, *Opt. Mater.*, 2016, **57**, 45–55.
- 35 C. A. Kodaira, H. F. Brito, O. L. Malta and O. A. Serra, *J. Lumin.*, 2003, **101**, 11–21.
- 36 R. D. L. Gaspar, E. M. Rodrigues, I. O. Mazali and F. A. Sigoli, *RSC Adv.*, 2013, **3**, 2794.
- 37 Q. Zhang, X. Wang, X. Ding and Y. Wang, *Inorg. Chem.*, 2017, **56**, 6990–6998.

